ELSEVIER

Nuclear Physics B (Proc. Suppl.) 113 (2002) 322–328

NUCLEAR PHYSICS B
PROCEEDINGS
SUPPLEMENTS

www.elsevier.com/locate/npe

Performance of the Transition Radiation Detector of the PAMELA space mission

M. Ambriola[a]*, on behalf of the PAMELA Collaboration

[a]University of Bari and INFN – Sezione di Bari,
Via Amendola 173, 70126 Bari, Italy

The performance of the Transition Radiation Detector (TRD) of the PAMELA telescope has been studied using beam test data and simulation tools. PAMELA is a satellite–borne magnetic spectrometer designed to measure particles and antiparticles spectra in cosmic rays. The particle identification at high energy will be achieved by combining the measurements by the TRD and a silicon–tungsten imaging calorimeter. The TRD is composed of 9 planes of straw tubes, interleaved with carbon fiber radiators. A prototype of the detector has been exposed to particle beams of electrons, pions and muons of various momenta at the CERN-PS and SPS accelerator facilities. In addition a dedicated Monte Carlo code has been developed to simulate the detector. Here we illustrate both simulation results and experimental data analysis procedures and we will discuss the estimated TRD performance.

1. INTRODUCTION

PAMELA is a satellite–borne magnetic spectrometer that has been designed to study the composition and energy spectra of the cosmic rays, with special focus on the antiparticle component ($\bar{p}$ and e^+). The search of antimatter is important to understand the origin and propagation mechanisms of cosmic rays in the Galaxy. Although the latest results [1–3] are in agreement, within the experimental accuracies, with a secondary origin of the cosmic ray antiprotons and positrons, a primary component cannot yet be ruled out, and the measurements need to be extended to a larger energy interval. PAMELA will allow to perform measurements of the energy spectra of $\bar{p}$ and e^+ with unprecedented statistics over the energy ranges, respectively, from 80 MeV up to 190 GeV and from 50 MeV up to 270 GeV. In addition it will search for light antinuclei, with a sensitivity of 10^{-7} in the $\overline{He}/He$ ratio, and perform measurements of the spectra of electrons and light nuclei, up to Z=6.

A scheme of the PAMELA instrument is shown in Fig. 1: it consists of a magnet spectrometer equipped with a permanent magnet and a

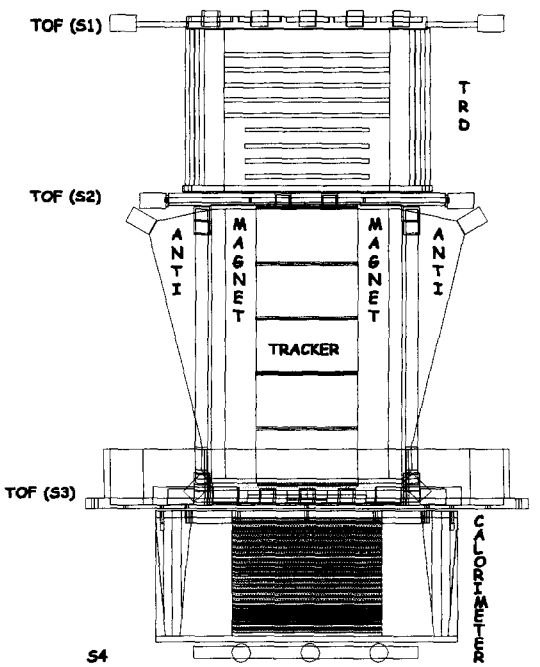

Figure 1. Schematic view of PAMELA instrument.

*ambriola@ba.infn.it

PII S0920-5632(02)01859-5

microstrip silicon tracker [4], a scintillator time-of-flight (TOF) device, a transition radiation detector (TRD) [5], a silicon tungsten imaging calorimeter [6], scintillator anti-coincidence (ANTI) counters [7] and a further scintillator counter (S4). A more detailed description of the PAMELA experiment is described elsewhere in these proceedings [8].

2. TRD DESIGN

The identification of positrons in cosmic rays requires a rejection factor against protons better than 10^{-5}. This high sensitivity will be reached using a combined selection by the calorimeter and the TRD. The TRD has been designed to reach a proton rejection factor of the order of 5% at a positron efficiency of about 90% in the PAMELA range of investigation.

The PAMELA TRD will be located at the top of the PAMELA apparatus, between two TOF layers (S1, S2).

The detector has a modular structure: the basic component is a straw tube, 28 cm long, 4 mm in diameter, made out of a 30 μm thin, copper–coated kapton foil. A tungsten anode wire, 25 μm in diameter, is placed inside the tube and stretched to a tension of $\sim$ 60 g. In order to have an efficient transition radiation photon conversion, each straw tube is filled with a gas mixture of Xe–CO_2 (80%–20%), working at a voltage of 1400 V in proportional mode.

Sixteen straw tubes are arranged sideways in a layer. Two of these layers are glued in a close–pack configuration to form a module of 32 straws. An artistic view of this module is shown in Fig. 2. A detection plane is formed housing three or four of these modules, depending on the plane position.

Radiator layers, composed of carbon fibers packed with a density of 60 g/l, are placed in the space between two consecutive detector planes while a double radiator layer is placed over the first detection plane.

The full TRD has an upside-down truncated pyramid shape, made of 10 radiator layers and 9 detector planes, for a total of 1024 straw tubes.

The TRD front–end electronics is based on charge integration technique. The straw signal is read–out by a CR1.4P VLSI ASIC chip [9], which has 16 channels. Each channel is composed by a charge sensitive preamplifier, a shaping amplifier, a track–and–hold circuit and input and output multiplexers. The chip output is converted by a 12–bit ADC. Finally the read–out electronics has the task of collecting and analyzing the data, using a DSP, prior to transmit them to the main CPU.

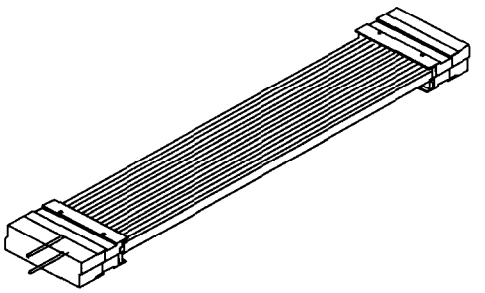

Figure 2. Artistic view of a 32 straw module.

3. BEAM TESTS AND DATA ANALYSIS

Prototypes of the PAMELA calorimeter, tracker and TRD detectors have been tested at CERN PS and SPS facilities. A full length TRD prototype of 10 radiators and 9 modules of straw tubes was equipped with a front–end board housing the CR1.4P chip and controlled by a DSP board. The calorimeter prototype, used in these tests, consisted of 6 silicon sensitive layers, each segmented along the X–direction, interleaved with 17 tungsten converters. Prototypes of the tracker, the anti-coincidence counters and the bottom scintillator counter were also present. All these detectors were aligned with a trigger system composed of scintillator paddles. A veto scintillator paddle was used for rejecting multiple tracks and restricting the beam geometry. During the test at the PS and SPS facility,

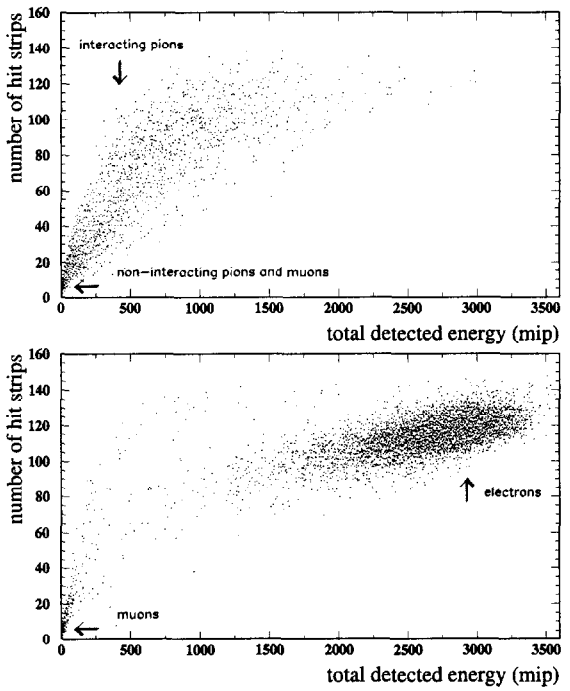

Figure 3. Number of hit strips versus the total detected energy in the calorimeter for 80 GeV/c pions (top) and electrons (bottom).

pion and electron beams were selected in the momentum ranges from 2 to 5 GeV/c and from 40 to 80 GeV/c, respectively. In both cases the beam contamination was not negligible; the worst case was found in the SPS beam due to the presence of muons in the SPS beam for momentum greater than $\sim$ 70 GeV/c. For this reason, a combined analysis of the TRD and calorimeter data was performed.

A data reduction procedure consisting of pedestal subtraction and common noise correction has been applied on each data sample. In order to select single particles crossing the TRD, a track reconstruction algorithm was implemented. The track was reconstructed for each event having a minimum of 4 layers hit. Then a fiducial area of 5 straws, centered on the reconstructed track, was defined and only hits in this area were considered for the analysis.

In order to reduce the beam contamination in the measured samples, the information from the calorimeter has been used for particle identification during the offline analysis. Depending on the particle momentum and type, cuts, optimized on simulated data, were applied on the distributions of the number of hit strips versus the total detected energy in the calorimeter. An example of the different classes of events are shown in Fig. 3 for a particle momentum of 80 GeV/c.

Following these steps, clean samples of radiating and non–radiating particles have been selected in order to study the TRD rejection power. In particular, electrons, having a Lorentz factor γ above the saturation value ($\gamma_{sat} \sim 3600$) at all values of energy considered in this work, were used as radiating particles, while pions as non–radiating particles.

4. TRD SIMULATION

A Monte Carlo simulation of the PAMELA TRD has been performed using the GEANT3.21 package, interfaced to the GARFIELD program and to a custom code. The latter was used to reproduce the transition radiation emission in the radiator, the absorption in the radiator materials and straw walls and the photon conversion in the gas mixture.

For relativistic particles, the transition radiation consists of X–ray photons which are emitted at small angles about the propagation direction of the particle generating the radiation. Therefore, the signals collected by the tubes may contain a contribution due to transition radiation conversion in addition to the ionization loss of the particle.

Consequently the model implemented for the production of the transition radiation is based on the 'field transport approach'. This approach is also used in the simulation [10] of the ATLAS TRT experiment. In this model, the transition radiation spectrum in the radiator is produced according to a calculation [11], as a function of the track length in the radiator and γ of the particle. A regular structure of the radiator, made of a stack of carbon foils of a given thickness regu-

larly spaced, has been assumed in the simulation. A correction factor for considering the irregular structure of the radiators in the detector has been introduced, as described later.

The algorithm takes into account the absorption of the radiation in the radiator itself, in the material between the radiators and in the sensitive region of the straw tube. As a result, the low–energy X–ray spectrum is suppressed while the region at high energy is increasingly transmitted. The portion of the transmitted transition radiation spectrum, which is expected to be converted in the gas mixture of the straw tube, is then computed using tabulated X–ray absorption cross sections. The number of converted X–ray photons is extracted from a Poisson probability distribution, having the value of the integral of this spectrum as mean. Since the radiator geometry is not regular (the carbon fibers are not regularly spaced), a tunable reduction factor has been applied to the amount of transition radiation produced, to take into account this difference [12]. The energy of these photons is then computed, based on the energy spectrum converted in the sensitive gas.

The ionization energy loss of fast charged particles in thin layers of gas is better described by the Photo–Absoption Ionization model (PAI) [13] than the Landau theory. The PAI model considers the atomic structure of the atoms to describe the energy loss distribution. Since the ionization process in thin gas layers is not adequately included in the GEANT3.21 package [14], the HEED program, interfaced to GARFIELD [15], was preferred in simulating the ionization energy loss in the TRD gas mixture.

The response of the TRD to ionization process in the sensitive gas has been studied by measured and simulated non–radiating pions. A best fit procedure with a Landau's function has been applied to the energy distribution detected in each TRD plane with simulated and experimental pions of the same momentum. The mean value of the maximum of these fitted curves has been used to normalize the experimental beam–test data of pions of 2 GeV/c (PS data) and 40 GeV/c (SPS data) to the simulated ones, allowing an energy calibration.

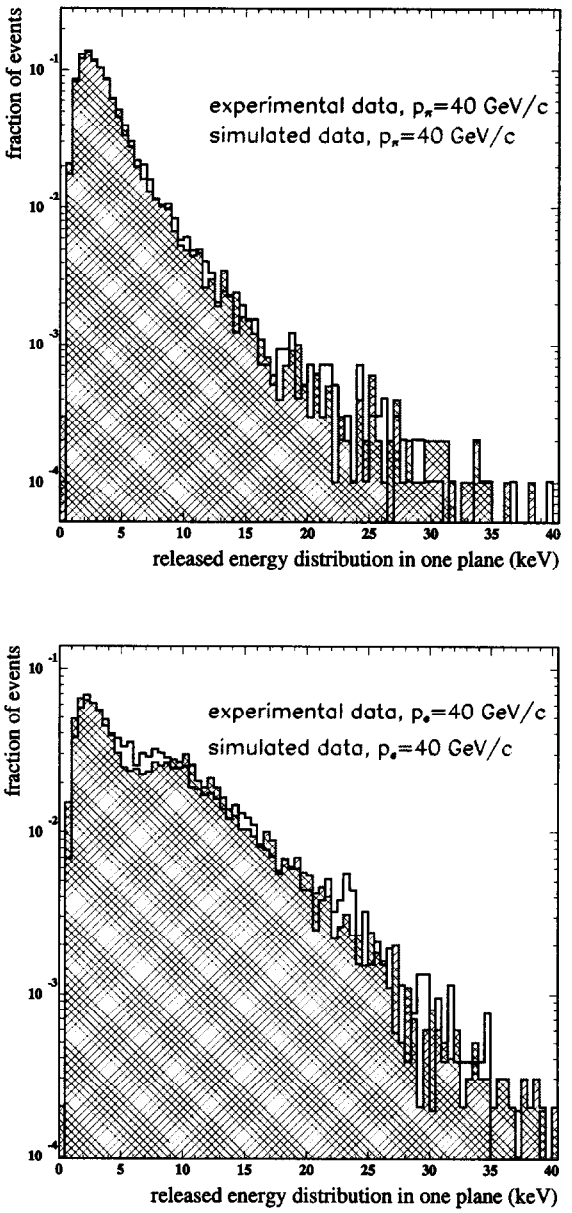

Figure 4. Distribution of the energy detected in a plane of the TRD from 40 GeV/c pions (upper plot). Distribution of the energy detected in a plane of the TRD for 40 GeV/c electrons (lower plot). The contribution of the transition radiation is clearly visible in addition to ionization above about 4 keV.

The upper plot of Fig. 4 shows a comparison between the distributions of simulated energy loss (hatch) and measured energy in a TRD plane for 40 GeV/c; here, the measured energy is after the energy calibration of the detector. The good agreement between the two distributions demonstrates the accuracy of the simulation to reproduce the ionization process. The lower plot of Fig. 4 shows the same comparison for 40 GeV/c electrons. The agreement between the measured and the simulated distributions is again good and the small difference in the 4–10 keV region could be due to the different radiator structures.

5. TRD PERFORMANCE

The TRD hadron rejection power, defined as pion contamination versus the electron efficiency at a given hadron momentum, has been estimated using a likelihood method. It is based on the difference in the energy deposited in each TRD plane by hadrons and electrons, selected as single-track events passing the calorimeter cuts (see beam tests and data analysis paragraph). As shown in Fig. 4, the shoulder in the electron energy distribution is due to transition radiation and it is absent in the pion spectrum. The e^- - π^- separation, shown in Fig. 4, could be improved with the following likelihood indicator:

$$\log L_e = \log \frac{\prod_{i=1}^{n} P_e^i(E_i)}{\prod_{i=1}^{n} P_\pi^i(E_i)}, \qquad (1)$$

where $P^i_{e(\pi)}(E_i)$ is the probability of an electron (pion) to produce the detected signal between E_i and $E_i + \Delta E_i$, in the plane i. These probability distributions are estimated from electron (radiating) and pion (non-radiating) reference samples.

Using the likelihood distributions, calculated by the equation (1), it was possible to study the pion contamination as a function of the electron efficiency. It was done by varying the cut on the value of $\log L_e$ to define the accepted electron class.

The curves of Fig. 5 show the pion and muon contamination versus electron efficiency for the PS (upper plot) and SPS (lower plot) data. As expected, pions of few GeV/c can be rejected to a level of about 5% at an electron efficiency of 90%.

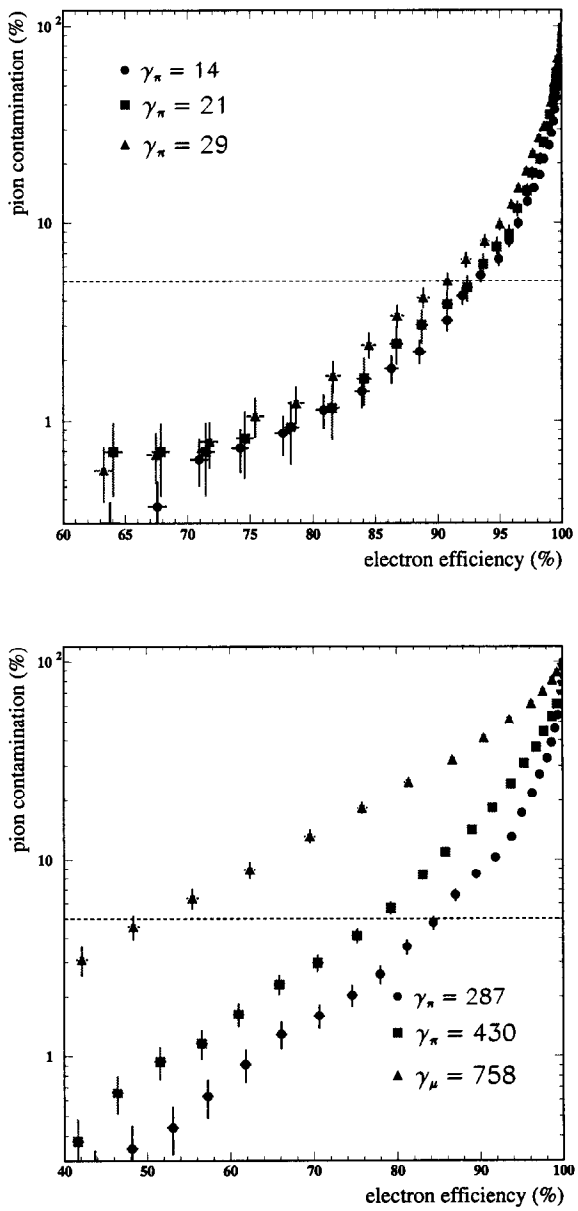

Figure 5. Pion contamination versus electron efficiency for the PS data (upper plot). Pion and muon contamination versus electron efficiency for the SPS data (lower plot).

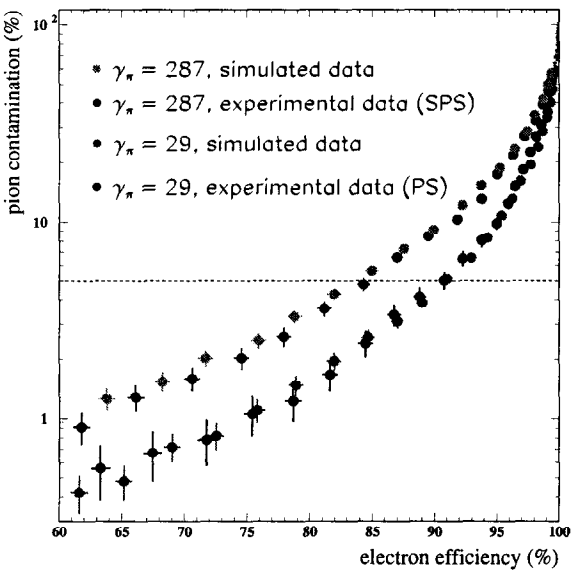

Figure 6. Measured pion contamination versus electron efficiency, compared to the Monte Carlo simulation.

At higher momenta, the relativistic increase of ionization losses of pions and muons slightly degrades the detector performance. As shown in the lower plot of Fig. 5, at a large enough value of particle energy the TRD starts to detect transition radiation from muons (triangles), as expected. The pion contamination versus the electron efficiency has been estimated also with simulated data, both for the PS and SPS momentum ranges of measurement. As an example, Fig. 6 shows that the TRD performance, calculated with measured pions of 3 (γ = 29) and 40 GeV/c (γ = 287), is well reproduced by the Monte Carlo simulation.

6. CONCLUSIONS

A full length prototype of the PAMELA TRD has been tested at CERN PS and SPS facilities along with prototypes of the other PAMELA detectors.

A TRD Monte Carlo has been developed and extensively compared to experimental data. The transition radiation simulation has been fine tuned using beam–test data. Besides we have verified that the simulation of the ionization describes accurately the data.

The results of a combined analysis of the signals from the TRD and calorimeter have shown that the performance comply with the design specifications. A rejection factor of the order of 5% for non–radiating particles is obtained at an electron efficiency of about 90%. The detector is thus capable of discriminating positrons from protons in cosmic rays at the required sensitivity. The prototype of the TRD has been exposed again to particle beams of even higher energy at SPS in June 2002. The analysis of these data is in progress.

REFERENCES

1. M. Boezio *et al.*, Astrophys. J. **561** (2001) 787.
2. M. Boezio *et al.*, Astrophys. J. **532** (2000) 653.
3. S. Orito *et al.*, Phys. Rev. Lett. **84** (2000) 1078.
4. O. Adriani *et al.*, Proc. 26^{th} ICRC (OG.4.2.10), Salt Lake City, 1999.
5. P. Spinelli, Proc. TRDs for the 3rd millenium, Giovinazzo-Bari (Italy), Frascati Physics Series **XXV** (2001) 177.
6. M. Boezio *et al.*, Nucl. Instrum. and Meth. **A487** (2001) 139.
7. J. Lund and M. Pearce, Proc. 7^{th} Int. Conf. on Advanced Technology and Particle Physics, Como, 2001.
8. M. Pearce *et al.*, The Status of the PAMELA spectrometer, these proceedings.
9. J. H. Adams *et al.*, Proc. 26^{th} ICRC (OG.4.1.18), Salt Lake City, 1999.
10. P. Nevski, Proc. Int. Europhysics Conf. on High Energy Physics, Marseille (1993) 386.
11. M. L. Cherry *et al.*, Phys. Rev. **D10** (1974) 3594.
12. M. Ambriola, Studio delle prestazioni del TRD della missione spaziale PAMELA, Ph.D. Thesis (2001), Università degli studi di Bari, http://wizard.roma2.infn.it/pamela/.

13. J. H. Cobb *et al.*, Nucl. Instr. and Meth. **145**, (1976) 315.
14. J. Apostolakis *et al.*, Nucl. Instr. and Meth. in Phys. Res. **A453** (2000) 597.
15. R. Veenhof, User's guide: 'Simulation of gaseous detectors', Garfield Version 7.04, http://garfield.web.cern.ch/garfield.